

# (An)Isotropy in Pantheon+ and Type Ia supernova samples: intrinsic limits of directional tests.

A. Quintana-Estellés<sup>1,2\*</sup> and P. Ruiz-Lapuente<sup>1,2</sup>

<sup>1</sup> Instituto de Física Fundamental, Consejo Superior de Investigaciones Científicas, c/. Serrano 121, E-28006, Madrid, Spain

<sup>2</sup> Institut de Ciències del Cosmos (UB-IEEC), c/. Martí i Franqués 1, E-08028, Barcelona, Spain

Received May , 2026

## ABSTRACT

**Context.** The use of methods that investigate the value of the Hubble constant  $H_0$  in different patches ( $60^\circ$  or  $90^\circ$  size) across the sky to probe the statistical isotropy of the Universe using large SNe Ia databases has led to contradictory claims of either anisotropy or isotropy. The anisotropy directions vary amongst research works.

**Aims.** The objective of this paper is to clarify the abovementioned claims and study the lack of basis for depicting directions of anisotropy with the present SNe Ia samples. We explain the type of limitation embedded in the SN Ia lightcurve method to determine the isotropy of  $H_0$  and the corresponding consequences.

**Methods.** The widely used analysis through the Region Fitting and the Hemisphere Comparison methods is done here using the Pantheon+ database, simulating 2000 distinct directions in the sky within a Bayesian Markov Chain Monte Carlo approach. We also study a smaller SNe Ia database, the Carnegie Supernova Project sample, leading to a similar kind of result as that from the Pantheon+ sample. We investigate the validity of the directions found for anisotropy within these analyses.

**Results.** We have found that within the tests used here, the Region Fitting method and the Hemisphere Comparison method, one can not determine with robustness the direction of an anisotropy of  $H_0$  using the present SNe Ia large data samples. This is intrinsic to the way  $H_0$  is obtained with the SNe Ia lightcurve method.

**Conclusions.** Achieving robust constraints will require a quite uniform sky coverage from larger SNe Ia samples with improved systematics.

**Key words.** Isotropy – Cosmological Principle – Hubble parameter – Supernovae

## 1. Introduction

Type Ia supernovae (SNe Ia) at high  $z$  led to the discovery of the acceleration of the Universe (Riess et al. 1998; Perlmutter et al. 1999) and dark energy. Large compilations of SNe Ia have recently suggested a tentative evolution in time of such unknown major component of the energy density of the Universe (Rubin et al. 2025; DESyr5, DESI<sup>1</sup>).

Apart from this use in cosmology, a puzzle emerged some years ago and still requires an explanation: the expansion rate of the Universe today, as obtained from SNe Ia calibrated with Cepheids, gives a value of  $H_0$  higher than that measured from the Cosmic Microwave Background (CMB). The value of  $H_0$  derived from the CMB is  $67.4 \pm 0.5 \text{ km s}^{-1} \text{ Mpc}^{-1}$  (Planck Collaboration 2020) and the *SHOES* value of  $H_0 = 73.3 \pm 0.9 \text{ km s}^{-1} \text{ Mpc}^{-1}$  (Murakami et al. 2023) had a discrepancy at the  $5.7\sigma$  level or even at the  $6\sigma$  level (Riess et al. 2025). The most recent results from polarization of the CMB obtained by the Third-Generation camera for the South Pole Telescope (SPT-3G) (Camphuis et al. 2026)

report a Hubble constant of  $H_0 = 66.66 \pm 0.60 \text{ km s}^{-1} \text{ Mpc}^{-1}$ ,  $6.2\sigma$  away from local measurements from *SHOES*.

A question that already arose when debating on the acceleration of the expansion of the Universe (Riess et al. 1998; Perlmutter et al. 1999) was whether the FLRW metric, which is valid for an homogeneous and isotropic Universe, was a legitimate assumption. If that was not the case, the findings from cosmological SNe Ia would be compromised. This had prompted interest in testing whether the Universe is isotropic and homogeneous on large scales ( $> 260 \text{ h}^{-1} \text{ Mpc}$ ) matter being evenly distributed and with no preferred directions. That would fulfill the Cosmological Principle (CP) and justify the assumption of the  $\Lambda$ CDM metric. For this, bulk flows arising from matter structure distribution which generates peculiar velocity fields should not exceed the  $\Lambda$ CDM expectations on scales of  $> 260 \text{ h}^{-1}$ . There are plenty of research works addressing whether this is the case. We refer here to Di Valentino et al. (2025), and references therein, for a complete update and discussions on this topic. We also refer to the review on large-scale peculiar velocities in the universe by Tsagas, Perivolaropoulos and Asvesta (2026). Recently, Lopes et al. (2024) have determined, using Pantheon+ SNe Ia, a bulk flow motion towards a direction close to the Shapley supercluster of  $132.14 \pm 109.3 \text{ km s}^{-1}$  in velocity at the effective distance of  $102.83 \pm 10.2 \text{ Mpc}$ .

\* Corresponding author: antonio.quintana@iff.csic.es

<sup>1</sup> DESyr5 stands for "Dark Energy Survey year 5", DESI for "Dark Energy Spectroscopic Instrument", SHOES for "Supernova  $H_0$  for the Equation of State of Dark Energy".

Such motion would be still consistent with the  $\Lambda$ CDM model. However, larger motions have been claimed at other effective distances by Watkins et al. (2023), Whitford et al. (2023) using the Cosmic-Flows4 (Tully et al. 2023). The samples used in those three research works of the Cosmic-Flows4 project are much larger than those from SNe Ia. Though, at present systematics seems to be reevaluated.

The debate both on the isotropy of the Hubble flow and on the compatibility of cosmic flows uses a variety of methods. A large number of tests use distance indicators to examine this question, such as the Tully-Fisher (T-F) relation, the Fundamental Plane (F-P) relation, the Surface Brightness Fluctuations (SBF), Type Ia supernovae (SNe Ia) and Type II SNe (SNe II). We will examine the part of Type Ia SNe, often used on their own.

The use of approaches that investigate the value of the Hubble constant  $H_0$  or the deceleration parameter  $q_0$  in different patches ( $60^\circ$  or  $90^\circ$  size) across the sky to probe the statistical isotropy of the Universe has led in some cases to claims of anisotropy and isotropy. There has not been consensus on this matter using different cosmological SNe Ia databases. Many authors have used the Pantheon+ database (Scolnic et al. 2022; Brout et al. 2022) to perform these tests (Bengaly, Alcaniz & Pigozzo 2024; Mc Conville & Colgáin 2023). Earlier works had used smaller samples such as the Pantheon (Scolnic et al. 2018) in Zhao, Zhou & Chang (2019); the Constitution sample (Hicken et al. 2009) in Kalus et al. (2013); the Union 2 sample (Amanullah et al. 2010) in Antoniou & Perivolaropoulos (2010) and in Colin et al. (2011); the Joint Light-Curve Analysis (JLA) (Betoule et al. 2014) in Deng & Wei (2018). Independently of the results, that could depend on the amount of SNe Ia in the database, there is the question of the nature of the scatter in those samples which has a very important effect in the validity of these approaches.

We start from the real uncertainty of the individual  $H_0$  measurements in Pantheon+ (Brout et al. 2022; Scolnic et al. 2022) samples. The point to point variation of  $H_0$  in the Pantheon+ sample and in other SNe Ia samples is basically of the order of  $8\text{--}9 \text{ km s}^{-1}$ . Part of this error is due to an intrinsic limitation of the SNe Ia light curve method to determine distances, which is of  $\sigma_{int} = 0.11 \text{ mag}$  (see for instance Mandel, Narayan & Kirshner 2011). This limitation in the method accounts for a  $4 \text{ km s}^{-1} \text{ Mpc}^{-12}$ . But, in fact, the larger variation, of the order of  $8\text{--}9 \text{ km s}^{-1} \text{ Mpc}^{-1}$ , is due to other errors such as the anchor in Cepheids (where in fact there could be an anisotropy in the absolute calibration of the period–luminosity relation of the Cepheids, given their low number of calibrators) or other factors such as the effect of existing peculiar velocities affecting SNe Ia.

<sup>2</sup> An error of  $\sigma_\mu = 0.11 \text{ mag}$  would result, for a value of  $H_0 = 73 \text{ km s}^{-1} \text{ Mpc}^{-1}$ , very approximately in an error in  $H_0$  of  $3.7 \text{ km s}^{-1} \text{ Mpc}^{-1}$ , irrespective of the distance. This limit is calculated from the following:

$$\sigma_{H_0} = H_0 \sqrt{\left(\frac{\sigma_z}{z}\right)^2 + \left(\frac{\sigma_D}{D}\right)^2}.$$

If we dismiss, for being close to 0,  $\frac{\sigma_z}{z}$ , then  $\sigma_{H_0} \sim H_0 \left(\frac{\sigma_D}{D}\right)$  and the error in D is :

$$\sigma_D = \frac{1}{5} \ln(10) \sigma_\mu D. \text{ This gives:}$$

$$\sigma_{H_0} \sim \frac{1}{5} \ln(10) \sigma_\mu H_0$$

We show here the effect that such  $H_0$  point to point variation has, even considering only the intrinsic error of the light curve method, in the analysis of the anisotropy of  $H_0$  in the sky and in the direction of such anisotropy. We do this with the Pantheon+ sample and compare it with research that has not taken this effect into account. We show the effect, as well, in a smaller but carefully treated SNe Ia sample as that of the Carnegie Supernova Project (Freedman et al. 2019).

Thus, we study the pattern in the measurement of  $H_0$  across the sky and test the ability to point to anisotropies using the SNe Ia samples. We examine the anisotropy/isotropy claims done so far to shed light on this important question.

This paper is structured as follows. In section 2, we present a comprehensive overview of the Pantheon+ sample, illustrating its distribution in Galactic coordinates and in redshift. This section introduces the framework for inferring cosmological parameters from the luminosity data of SNe Ia. We describe in detail our methodology in section 3. The main results are presented in sections 4 and 5. In section 6 we provide the corresponding discussion, and we conclude with our findings in section 7.

## 2. Pantheon+ dataset

We explore the Pantheon+ sample (Brout et al. 2022; Scolnic et al. 2022), which includes 1701 light curves of 1550 distinct SNe Ia from 18 different surveys, confirmed through spectroscopy and with redshifts ranging  $0.001 < z < 2.26$ . This sample can be used as it is or in combination with SH0ES results (Riess et al. 2022). When combined, the inclusion of 42 Cepheids distance measurements, in the same host galaxies as some supernovae, enables the calibration of the absolute magnitude of SNe Ia using the cosmic distance ladder method. We show in Figure 1 the SNe Ia distribution in Galactic coordinates and that in redshift in Figure 2.

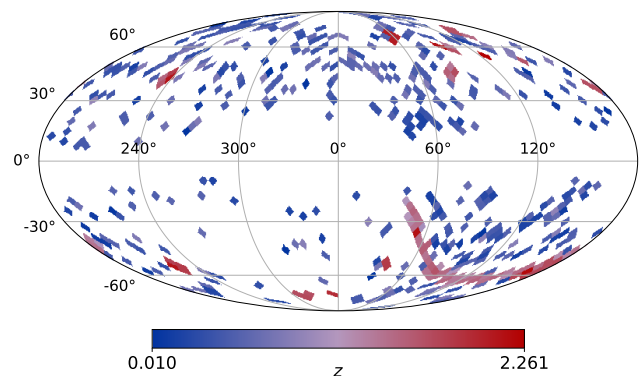


Fig. 1: SNe Ia distribution in galactic coordinates, with the color bar representing their redshift.

$\chi(z_{\text{cmb}})$  is the comoving distance, defined as:

$$\chi(z_{\text{cmb}}) = \int_0^{z_{\text{cmb}}} \frac{dz}{H(z)} \quad (1)$$

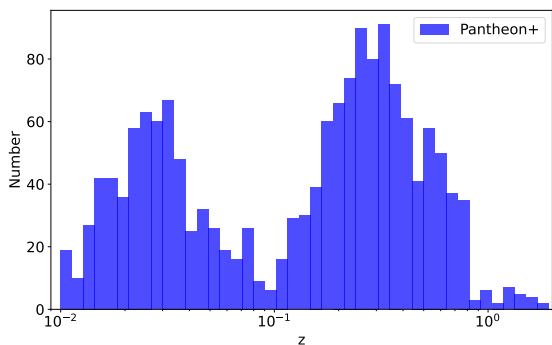


Fig. 2: Redshift histogram for Pantheon+ dataset.

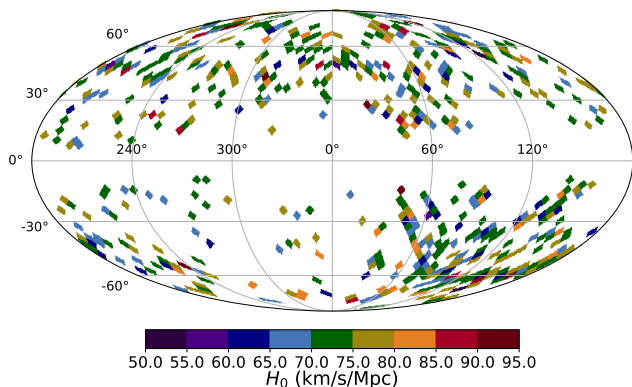


Fig. 3: Individual  $H_0$  values derived by inverting the distance–redshift relation for SNe Ia. Pantheon+ dataset.

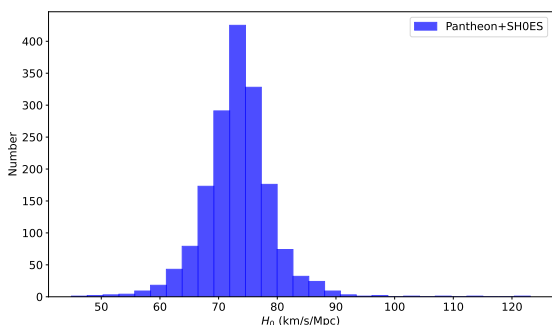


Fig. 4: Histogram of individual  $H_{0,i}$  values.

More interestingly, we present in Figure 3 the Hubble constant ( $H_0$ ) values computed for individual SNe Ia using Pantheon+, by inverting the distance–redshift relation using the original dataset values. The luminosity distance is derived from the distance modulus, and  $H_0$  is calculated assuming a second-order cosmographic expansion in redshift, with fixed deceleration and jerk parameters,  $q_0 = -0.55$  and  $j_0 = 1.0$ . This approach yields a preliminary local estimate of  $H_0$  for each SN Ia ( $H_{0,i}$ ), enabling visualization of its directional distribution. We observe that the resulting  $H_0$  values,  $H_{0,i}$  appear to be distributed in a seemingly random manner, with no apparent trend or structure. Moreover, the individual  $H_{0,i}$  values exhibit a considerable spread, ranging from 50 to almost 100  $\text{km s}^{-1} \text{Mpc}^{-1}$  (see Figure 4).

We start by introducing the fundamental relationship between the luminosity distance,  $D_L$ , and the expansion his-

tory,  $H(z)$ . For a spatially flat universe, this relationship is expressed by equation 2:

$$D_L(z_{\text{hel}}, z_{\text{cmb}}) = (1 + z_{\text{hel}}) \frac{c}{H_0} \chi(z_{\text{cmb}}) \quad (2)$$

where  $c$  is the speed of light;  $H_0$  is the Hubble constant;  $z_{\text{hel}}$  is the heliocentric redshift;  $z_{\text{cmb}}$  is the redshift in the CMB frame due to the expansion of the universe, with  $H(z)$  depending on the underlying cosmological model. For a Flat- $\Lambda$ CDM model, it takes the form:

$$H(z) = H_0 \sqrt{\Omega_m (1+z)^3 + (1 - \Omega_m)} \quad (3)$$

where  $\Omega_m$  is the matter density parameter. The observed distance modulus,  $\mu_{\text{obs},i} = m_i - M$ , for each SN Ia is defined in terms of its apparent magnitude,  $m_i$ , and absolute magnitude,  $M$ , which is degenerate with  $H_0$ . This degeneracy can be removed by using distance measurements to Cepheids located in the same host galaxies as the SNe Ia, as provided by SH0ES (Riess et al. 2022). For Pantheon+ the observed distance moduli are estimated using equation (1) from Brout et al. (2022).<sup>3</sup>

Pantheon+ has been crucial in the development of tests of cosmic isotropy and in attempts to describe cosmic bulk motions. However, the limitation in the method of  $4 \text{ km s}^{-1} \text{Mpc}^{-1}$  in  $H_{0,i}$  confines as well the possibility to determine bulkflows. It is possible to determine them at low  $z$ , but as  $z$  grows the constraint from  $H_{0,i}$  needs a larger bulk flow to be detected. This can be seen from the relation between peculiar velocities, luminosity distance  $D_L$  and  $H_0$ :

$$\sigma_{v_{\text{pec}}} = \frac{1}{\sqrt{2}} \sqrt{D_L^2 \sigma_{H_0}^2 + H_0^2 \sigma_{D_L}^2} \quad (5)$$

The value of the Hubble flow in the sky, with the distribution of individual  $H_{0,i}$ , is a source for studying bulkflows at a very low  $z$ , but it is not so for larger  $z$ . The overall distribution of matter and the produced field of peculiar velocities leave imprints on  $H_0$  in all directions of the sky.

Here the full Pantheon+SH0ES dataset will be analyzed using the Region Fitting (RF) method (Hu et al. 2023) and the Hemisphere Comparison (HC) method (Schwarz and Weinhorst 2007). The RF method incorporates the full

<sup>3</sup>

For Pantheon+, the redshift used in equation 1 is the so-called *Hubble Diagram redshift* as defined in equation (7) of Carr et al. (2022), which accounts for both our motion relative to the CMB and the peculiar velocity of the source. The studies of Carr et al. (2022) are built upon the idea of replacing individual host galaxy redshifts with average redshifts of host galaxy groups (Peterson et al. 2022). Such redshift is:

$$z_{\text{HD}} = \frac{1 + z_{\text{CMB}}}{1 + z_p} - 1 \quad (4)$$

The *Hubble diagram redshift*  $z_{\text{HD}}$  requires knowledge of the SN host's peculiar redshift  $z_p$ . The  $z_{\text{CMB}}$  is the CMB redshift and  $z_p$  is the redshift corresponding to the peculiar velocity, which is modeled from peculiar velocity groups reconstruction by Peterson et al. (2022).

covariance matrix to account for both statistical and systematic uncertainties. For this dataset, we investigate the impact of the Cepheid calibrator subsample. That is, for any given region of the sky, we examine the effect of using either the full set of 42 Cepheid calibrators or only those located within the region under study. We additionally test whether the directions of maximum anisotropy are consistent with statistical noise and sample variance. Thus, given that the SNe Ia lightcurve method has an intrinsic error of residuals of  $\sigma_{int} \simeq 0.11$  mag, that corresponds to variations of approximately  $4 \text{ km s}^{-1} \text{ Mpc}^{-1}$  in  $H_0$ , we perform simulations to test whether the directions of maximum anisotropy remain stable under such variations in the distance modulus. We also apply the HC method to Pantheon+ and similarly explore the effect of the distance uncertainties on the results.

### 3. Methodology

Therefore, in order to compare observations with theory, the theoretical distance modulus for each SNe Ia, given its redshift,  $z_i$ , and a set of cosmological parameters,  $\Theta$ , is:

$$\mu_{th}(z_i, \Theta) = 5 \log_{10} \left( \frac{D_L(z_i, \Theta)}{\text{Mpc}} \right) + 25 \quad (6)$$

For Pantheon+, the best-fit of the cosmological parameters can be obtained by minimizing a  $\chi^2$  likelihood,  $\mathcal{L}$ , defined as:

$$-2 \ln(\mathcal{L}) = \chi^2 = \Delta\mu_i C_{ij}^{-1} \Delta\mu_j^T \quad (7)$$

where  $\Delta\mu_i = \mu_{obs,i} - \mu_{th}(z_i, \Theta)$ , and  $C_{ij}^{-1}$  is the inverse of the covariance matrix, which accounts for both systematic and statistical uncertainties, as well as the expected correlations among the SNe Ia within the sample when evaluating cosmological models. Each element of the covariance matrix represents the covariance between pairs of SNe Ia in the sample (Vincenzi et al. 2024).

The minimization of the  $\chi^2$  likelihood function is made using a Bayesian Markov Chain Monte Carlo (MCMC) approach. Among the tools used in this analysis, we employ the CosmoSIS framework (Zuntz 2015), a modular tool designed for cosmological parameter estimates that efficiently combines diverse computational methods. We use the `emcee` sampler for best-fit estimates<sup>4</sup> (Foreman Mackey 2013), where the  $\chi^2$  statistic serves as a measure of the goodness of fit. The MCMC samples are visualized using `getdist` (Lewis 2019). The mean of the marginalized posterior distributions is estimated for all fits, along with probability contours for 68.3% and 95.5%. The Pantheon+ data used in this work are publicly available on GitHub.<sup>5</sup>

During the fitting process, all model-dependent cosmological parameters are allowed to vary freely and are simultaneously fitted. The results are mapped within the galactic coordinate

<sup>4</sup> For the `emcee` fitting, we ensure that the total number of samples in the chain exceeds at least 50 times the autocorrelation function ( $N_{samples} / \tau > 50$ ) by using more than twice as many walkers as there are free parameters. The initial 20% of the chain is then discarded as burn-in.

<sup>5</sup> See Pantheon+: <https://github.com/PantheonPlusSHOES>.

system. For the main parameters of interest we adopt the same flat priors as those used by Brout et al. (2022), summarized in Table 2. It should be noted that for Pantheon+ these are the only free parameters.

Pantheon+	
$\Omega_m$	[0.1, 0.9]
$h$	[0.55, 0.91]
$M$	[-20.0, -18.0]

Table 1: Flat priors for the cosmological parameters in each dataset.

The idea behind the RF method is to generate multiple randomly distributed directions,  $(l_i, b_i)$ , which are then used to select SNe Ia within specific regions, forming distinct subsamples in which cosmological parameters are fitted for each sky direction. A region is defined by the condition  $\theta < \theta_{max}$ , where  $\theta$  is the screening angle, representing the angular separation between the random direction and the position of each SN Ia, with  $\theta_{max} = 90^\circ$  explored in the present study.

SNe Ia data located in respect to specific regions  $\theta < \theta_{max}$ , with  $l \in (0^\circ, 360^\circ)$  and  $b \in (-90^\circ, 90^\circ)$  being the longitude and latitude of the SN Ia in the galactic coordinate system and  $\mathbf{D}(\mathbf{l}, \mathbf{b})$  the vector direction between the SN Ia position and the selected  $\theta$ , form subsamples. In order to describe the degree of deviation from the cosmological principle, the anisotropic level  $AL$  is described as (see, for instance, Hu et al. 2024):

$$AL_{max} = \frac{h_{max} - h_{min}}{\sqrt{\sigma_{h_{max}}^2 + \sigma_{h_{min}}^2}} \quad (8)$$

Here,  $h$  is the dimensionless Hubble constant,  $h = H_0/100 \text{ km s}^{-1} \text{ Mpc}^{-1}$ ,  $h_{min}$  and  $h_{max}$  are the minimum and maximum  $h$  values of the best fitting results, with the corresponding  $\sigma_{h_{min}}$  and  $\sigma_{h_{max}}$   $1\sigma$  error.  $AL_{max}$  is calculated as well with a set of the original data spread evenly in the sky. In this isotropic data set,  $AL$  is also calculated. In this way, a better idea of the significance of the results is obtained.

We apply the RF method to the Pantheon+ dataset, analyzing 2000 distinct sky regions and using the full sample with a  $z > 0.01$  cut. This analysis is performed twice: first, using only the Cepheid calibrators located within each region; and second, using all 42 Cepheids to calibrate all regions. Performing both analyses allows us to separate underlying anisotropy signals from potential artifacts arising from variations in the availability or spatial distribution of calibrators, which are limited in number, examining whether the identified preferred directions are influenced by the calibration sample size and distribution. We report the statistical significance of the directions of maximum anisotropy obtained from both approaches. The uncertainties on the inferred directions are estimated from the standard deviation of the directions within  $30^\circ$  of angular separation from each preferred direction with their  $h$  values within  $1\sigma$ , which is chosen as a reasonable estimate to quantify local directional trends.

For Pantheon+, the availability of the full covariance matrix enables a statistically robust evaluation of significance through a Cholesky Decomposition of the covariance matrix of the data vectors corresponding to each pair of directions to be compared. This technique enables the proper application of the RF method by accounting for correlations between overlapping SNe Ia in different sky regions. The RF method extends and generalizes the HC method, originally proposed by Schwarz & Weinhorst (2007). The HC method basically differs from the RF in that the regions are hemispheres covering  $180^\circ$  degrees in the sky. The RF method is particularly well suited for the Pantheon+ dataset, where the full covariance matrix is available. The Cholesky Decomposition is a widely used technique in numerical linear algebra (Golub et al. 1996; Johnson et al. 2014; Chapra et al. 2017), particularly for Monte Carlo simulations and statistical modeling, where it is applied to simulate systems with multiple correlated variables (Asmussen 2007). The method requires that the covariance matrix be symmetric and positive-definite. By decomposing the covariance matrix into a product of a lower triangular matrix and its transpose, the decomposition allows the generation of correlated samples that preserve the underlying covariance structure. This process is mathematically represented as:

$$C = LL^T \quad (9)$$

where  $L$  is a lower triangular matrix. This factorization ensures that the covariance structure is retained, allowing for statistically robust inferences about systematic effects and uncertainties. Different applications of the Cholesky Decomposition can be found in the literature. So, for instance, Nikakhtar et al. (2018) use it to generate Monte Carlo realizations of correlated random walks, whereas Yuan & Eisenstein (2019) apply it to de-correlate covariance matrices in galaxy clustering analyses.

We further assess the robustness of the anisotropy directions derived from the Pantheon+ dataset by simulating observational residuals in the distance modulus. Following the representative distance-modulus uncertainties (corresponding to an approximate dispersion of  $4 \text{ km s}^{-1} \text{ Mpc}^{-1}$  in  $H_0$ ), we generate four simulated realizations of the Pantheon+ dataset in which each supernovae distance modulus is randomly perturbed by the  $\sigma_{int}$  of the SN Ia method.

$$H_{0,i\pm} = H_{0,i}(1 + \delta_i) = H_{0,i} + \delta H_{0,i} \quad (10)$$

The set of simulations considered (restricted by computational constraints) can identify instabilities: if significant directional variations are already observed under a small number of realizations, this should provide evidence that the inferred anisotropy directions are sensitive to observational uncertainties. This stability test is applied to the RF method and the HC method using local Cepheid calibrators within each sky region (as in the first approach described above). It is also applied using the full set of 42 Cepheids. For each method, we identify the new directions of maximum and minimum  $h$ . Shifts between the anisotropy directions in the original and simulated datasets will indicate whether the observed anisotropies are consistent with residual uncertainties.

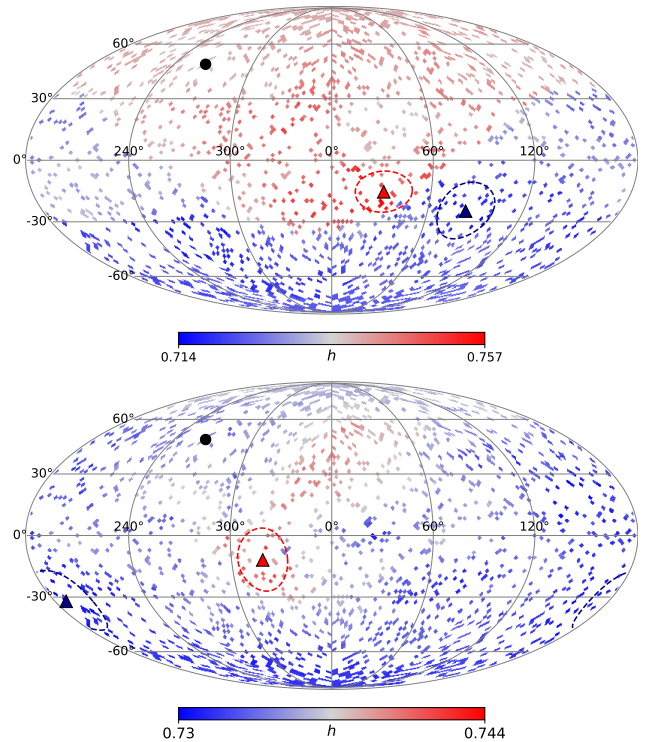


Fig. 5: RF method applied to Pantheon+ dataset with only directional Cepheid calibrators (top), and with all 42 Cepheids calibrators in all directions (bottom). Panel show all-sky maps of  $h$  for the 2000 directions investigated. Red and blue triangles mark the directions of maximum and minimum  $h$ , respectively. The black circle denotes the CMB dipole direction.

#### 4. Results from the Pantheon+ dataset

The RF method using local Cepheids to calibrate each region yields an all-sky map with  $h$  in the range 0.714 to 0.757, while using all 42 Cepheids for calibration produces a narrower range, from 0.730 to 0.744. For the local-Cepheid calibration, higher  $h$  values are observed across a broad region covering much of the northern galactic hemisphere, coinciding with the CMB dipole direction, whereas lower values appear in the southern hemisphere. This hemispherical contrast is significantly attenuated when all 42 Cepheids are used for calibration, as observed in Figure 5. In particular, for the RF method using only local Cepheid calibrators, we find:

$$h_{\max}^{\text{Local}} = 0.757 \pm 0.016, \quad h_{\min}^{\text{Local}} = 0.714 \pm 0.016,$$

at  $(l, b)_{h_{\max}^{\text{Local}}} = (31.4 \pm 17.2, -15.2 \pm 10)$  and  $(l, b)_{h_{\min}^{\text{Local}}} = (83.9 \pm 17.2, -24.6 \pm 14.1)$ , respectively.

When calibrating with all 42 Cepheids, the maximum and minimum values shift to:

$$h_{\max}^{\text{All}} = 0.744 \pm 0.011, \quad h_{\min}^{\text{All}} = 0.730 \pm 0.010,$$

at  $(l, b)_{h_{\max}^{\text{All}}} = (318.7 \pm 14.9, -11.7 \pm 15.3)$  and  $(l, b)_{h_{\min}^{\text{All}}} = (186.0 \pm 17.5, -32.2 \pm 15.2)$ , respectively.

Thus the preferred directions obtained with the two approaches differ. This suggests a dependence on the specific Cepheid sample considered. Since the second approach makes use of the full Cepheid dataset, it is expected to provide a more robust determination of the anisotropy directions and of the corresponding  $h$  variation estimates.

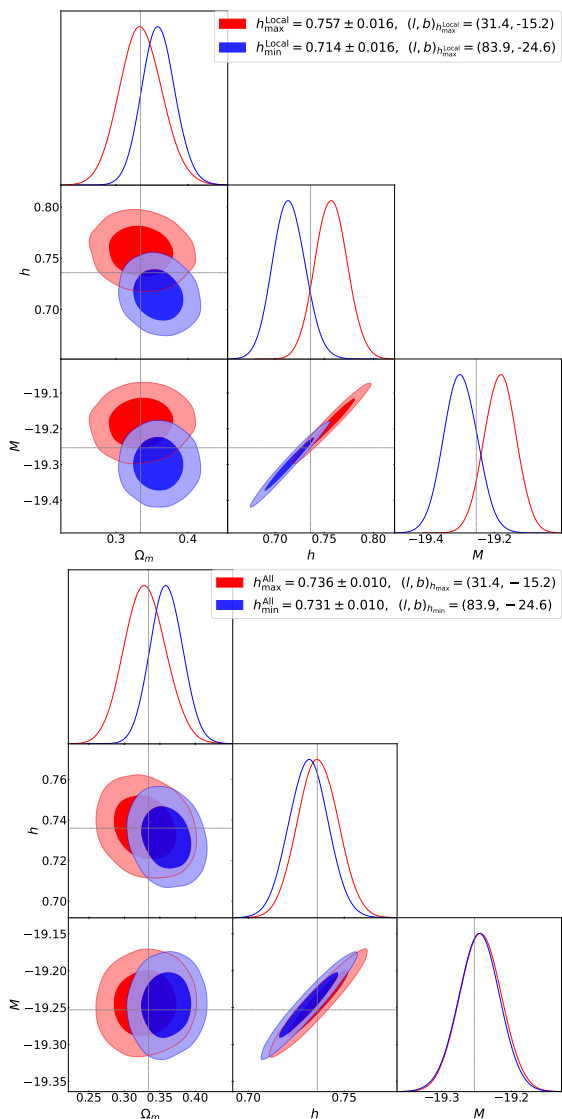


Fig. 6: Probability density contours for Pantheon+ with the RF method for the free parameters  $\Omega_m$ ,  $h$ , and  $M$ , in the specific directions  $(l, b)_{h_{\max}^{\text{Local}}} = (31.4 \pm 17.2, -15.2 \pm 10.0)$  and  $(l, b)_{h_{\min}^{\text{Local}}} = (83.9 \pm 17.2, -24.6 \pm 14.1)$ . Left: Using only local Cepheid calibrators. Right: Using all 42 Cepheid calibrators in both directions. Vertical and horizontal lines indicate the parameter values reported by Brout et al. (2022) from their analysis of the full Pantheon+ sample.

To evaluate the statistical significance of the maximum and minimum  $h$  values for each case, we apply the Cholesky Decomposition methodology described in Section 3. Starting from the covariance matrix of the combined Max+Min sample, we generate 100 realizations and perform the parameter inference for the combined, maximum, and minimum subsamples. From these simulations, we construct the distributions of the shifts with respect to the combined sample and

use their standard deviations to quantify the statistical significance of the observed differences. Using local Cepheids, the combined Max+Min sample yields  $h_{\text{Max+Min}}^{\text{Local}} = 0.732 \pm 0.013$ , with the statistical significance of the observed shifts being  $2.8\sigma$  for the maximum direction and  $1.8\sigma$  for the minimum. When calibrating with all 42 Cepheids, the combined sample gives  $h_{\text{Max+Min}}^{\text{All}} = 0.735 \pm 0.010$ , with the corresponding statistical significance of the maximum and minimum directions being smaller than  $1\sigma$  in both cases, as depicted in Table 2. One important finding is that the  $2.8\sigma$  significance of  $h_{\max}^{\text{Local}}$  found using only the local Cepheid calibrators disappears when all 42 Cepheids are used at the same direction, with the value shifting from  $0.757 \pm 0.016$  to  $0.736 \pm 0.010$ . Similarly, the  $1.8\sigma$  significance of  $h_{\min}^{\text{Local}}$  vanishes when evaluated with all Cepheid calibrators, changing from  $0.714 \pm 0.016$  to  $0.731 \pm 0.010$ . The corresponding corner plots for these two cases are shown in Figure 6.

To assess the robustness of the inferred anisotropy directions, we introduce random perturbations  $H_{0,i\pm} = H_{0,i}(1 + \delta_i)$ . We quote in Table 3 the results with the RF and HC where the whole or the local SNe Ia Cepheids have been considered.

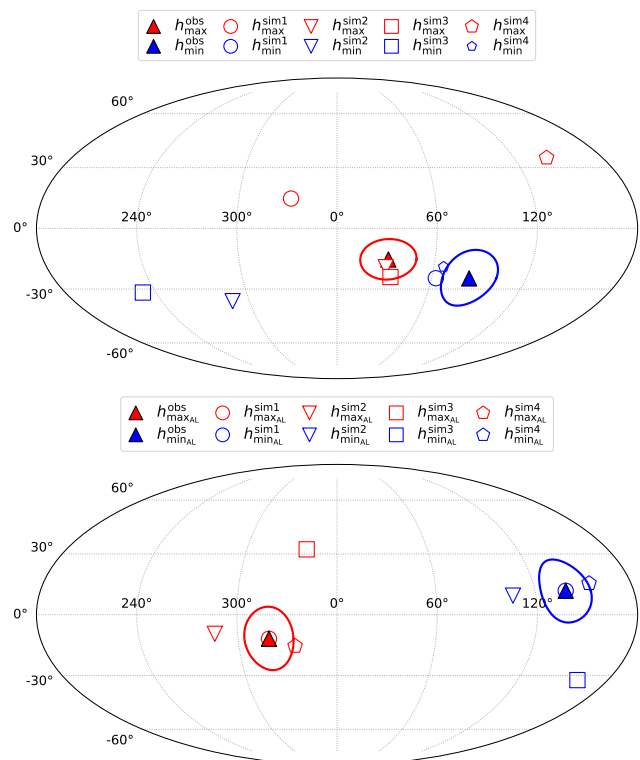


Fig. 7: Results of simulations including the intrinsic scatter of the SNe Ia method for Pantheon+. Top: RF method with local Cepheid calibrators; Bottom: HC method with all 42 Cepheids.

They are just reflecting the error in the SNe Ia lightcurve method, and therefore are smaller than Pantheon+ residual uncertainties, for both the RF method with local Cepheid calibrators and the HC method using all 42 Cepheids. In Table 3 we present four realizations of the Pantheon+ dataset with the applied perturbations for each approach. It can be seen that both maximum and minimum  $h$  values, as well as the corresponding preferred directions, differ in most cases from those obtained in the unperturbed case. In the case of

RF method	$h[\Delta h]$	Significance	A. direction ( $l, b$ )
<b>Local Cepheids</b>			
Max + Min	$0.732 \pm 0.013$	-	-
Max	$0.757 \pm 0.016$ [0.025]	$2.8\sigma$ in $h$	$(31.4 \pm 17.2, -15.2 \pm 10.0)$
Min	$0.714 \pm 0.016$ [-0.018]	$1.8\sigma$ in $h$	$(83.9 \pm 17.2, -24.6 \pm 14.1)$
<b>All 42 Cepheids</b>			
Max + Min	$0.735 \pm 0.010$	-	-
Max	$0.744 \pm 0.011$ [0.009]	$< 1\sigma$ in $h$	$(318.7 \pm 14.9, -11.7 \pm 15.3)$
Min	$0.730 \pm 0.010$ [-0.005]	$< 1\sigma$ in $h$	$(186.0 \pm 17.5, -32.2 \pm 15.2)$

Table 2: Hubble parameter estimates for Pantheon+ with the RF method. Top: using local Cepheids to calibrate each region; bottom: using all 42 Cepheids. This table reports the significance of  $h_{\max}$  and  $h_{\min}$  relative to the combined Max+Min sample, which denotes the reference dataset constructed by combining all SNe Ia belonging to the  $h_{\max}$  and  $h_{\min}$  regions, including those shared by both datasets. The cosmological parameters are fitted to this combined sample to obtain the reference value  $h_{\max+\min}$  between the two anisotropy directions. Since the  $h_{\max}$  and  $h_{\min}$  measurements are not independent of the combined sample due to the large overlap in SNe Ia, we quantify the significance of the shifts by generating 100 independent realizations of the full dataset for each case (local and all Cepheids) using a Cholesky decomposition of the full covariance matrix. For each realization, we estimate  $h_{\max+\min}$ ,  $h_{\max}$ , and  $h_{\min}$ , and compute the shifts  $\Delta h = h_{\max} - h_{\max+\min}$  and  $\Delta h = h_{\min} - h_{\max+\min}$ . The standard deviation  $\sigma(\Delta h)$  is then obtained from the distribution of simulated shifts, and the significance is defined as the ratio between the measured  $\Delta h$  and  $\sigma(\Delta h)$ . For example, in the local Cepheid case for the maximum direction, we find  $\Delta h = 0.025$  and  $\sigma(\Delta h) \simeq 0.00886$ , corresponding to a significance of  $\sim 2.8\sigma$ . This approach properly accounts for the correlations between subsamples and avoids an incorrect quadrature combination of uncertainties.

Table 3: RF method with local Cepheids and HC method with all 42 Cepheids, four intrinsic-scatter simulations ( $\sigma_{int} \simeq 0.11$  mag) for Pantheon+. Values of  $h$  corresponding to the maximum anisotropy and their associated directions are listed for each realization.

Method	N	$h_{\max}$	$(l, b)_{h_{\max}}$	$h_{\min}$	$(l, b)_{h_{\min}}$
RF Local Cepheids	1	$0.786 \pm 0.013$	(291.5, 25.2)	$0.695 \pm 0.017$	(65.8, -27.2)
	2	$0.785 \pm 0.018$	(58.0, -6.5)	$0.713 \pm 0.013$	(219.7, -25.4)
	3	$0.792 \pm 0.018$	(36.3, -20.2)	$0.679 \pm 0.015$	(230.0, -33.4)
	4	$0.752 \pm 0.013$	(142.1, 35.1)	$0.676 \pm 0.016$	(66.0, -18.8)
HC All Cepheids	1	$0.763 \pm 0.011$	(318.7, -11.7)	$0.745 \pm 0.010$	(138.7, 11.7)
	2	$0.748 \pm 0.011$	(286.2, -9.3)	$0.735 \pm 0.010$	(106.2, 9.3)
	3	$0.751 \pm 0.011$	(339.8, 32.4)	$0.736 \pm 0.011$	(159.8, -32.4)
	4	$0.733 \pm 0.010$	(334.3, -15.3)	$0.720 \pm 0.010$	(154.3, 15.3)

the RF method, the changes appear more irregular, reflecting lower stability in the inferred anisotropy directions. In contrast, for the HC method the directions do not vary in a completely random manner, but the maximum anisotropy directions tend to shift beyond the estimated uncertainty region. This suggests that neither method yields consistent anisotropy directions. Figure 7 shows the original preferred directions along with those obtained from the four perturbed realizations of the Pantheon+ dataset for each case.

## 5. The nature of the SNe Ia sets

Previously to the use of Pantheon+, as mentioned in the introduction, samples with smaller amounts of SNe Ia such as Union2, JLA, Constitution sample, amongst others, were used.

Those studies suggest that any anisotropy is expected to be more prominent at low redshift, and in particular Colin et al. (2019) find a significant dipolar anisotropy. In this context, the CSP sample, which is almost entirely composed of nearby SNe Ia, provides a useful dataset to explore potential anisotropy signals in the local Universe. The CSP dataset has notably fewer SNe Ia than Pantheon+ (342 SNe Ia) and the full covariance matrix is not available. This precludes the use of the RF method, but it remains testable with the

HC method. A similar limitation in the number of SNe Ia was present in the JLA sample (Betoule et al. 2014), for which isotropy analyses using the HC method have also been performed (Lin, Wang, Chang 2016; Deng & Wei 2018).

The CSP (Hamuy et al. 2006) combines observations from CSP-I and CSP-II, two consecutive campaigns which ran from 2004 to 2015. The CSP-II campaign extended its observations deeper into the Hubble flow, with its NIR spectroscopy program and overall survey strategy detailed in Phillips et al. (2019) and Hsiao et al. (2019). This dataset offers a homogeneously calibrated sample of SNe Ia, with distance scales anchored through Cepheids, Tip of the Red Giant Branch (TRGB), and Surface Brightness Fluctuations (SBF) calibrators. For consistency with the calibration approach adopted in Pantheon+, we base our analysis on the Cepheid-calibrated CSP sample in the B band maximum magnitudes. This sample contains SNe Ia including 25 hosts with Cepheid distances for anchoring the absolute magnitude, covering the redshift range up to  $z < 0.138$ . The calibration values and distance scale information are taken from Uddin et al. (2024), which presents the latest combined analysis of CSP-I and CSP-II data for  $H_0$  determination. When we look at the individual errors in  $H_0$  from the CSP SNe Ia we find as well  $8-9 \text{ km s}^{-1} \text{ Mpc}^{-1}$ , as it happens in Pantheon+. The part coming from the method is typically of  $4 \text{ km s}^{-1} \text{ Mpc}^{-1}$  coming from the intrinsic error of the

SN Ia lightcurve method. However, the larger variations, of the order of  $8\text{--}9 \text{ km s}^{-1} \text{ Mpc}^{-1}$ , are the final budget for each  $H_{0,i}$  determination (see, for instance, Ruiz-Lapuente et al. 2025).

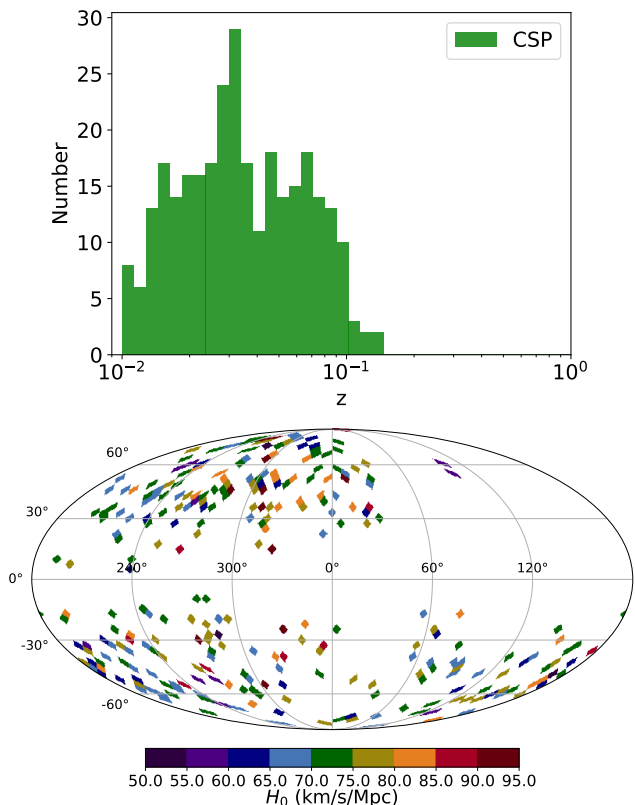


Fig. 8: Left: Redshift distribution of the CSP sample. Right: Distribution of SNe Ia in the sky, with the individual  $H_{0,i}$  of each SN Ia. As in the case of Pantheon+, we find variations of  $7\text{--}9 \text{ km s}^{-1} \text{ Mpc}^{-1}$  from one  $H_{0,i}$  to another one.

We show the redshift distribution in Figure 8 and the values of  $H_{0,i}$  for each CSP SN Ia in the sky.

We apply the HC method to the CSP sample using all the 25 Cepheid calibrators of the CSP in each direction. The all-sky map of the Hubble parameter shows  $h$  to be in the range 0.701 to 0.738. From Figure 9 it is observed that higher values of  $h$  are obtained over a broad region encompassing the CMB dipole direction, similarly to the Pantheon+ dataset. The HC method, for the CSP sample, when accounting only for statistical uncertainties, yields a maximum anisotropy level of  $2.7AL$  in  $h$  between the opposite directions  $(l, b)_{h_N} = (354.5 \pm 12.2, 6.9 \pm 15.1)$  and  $(l, b)_{h_S} = (174.5 \pm 12.2, -6.9 \pm 15.1)$ , corresponding to the values

$$h_N = 0.737 \pm 0.009, \quad h_S = 0.703 \pm 0.009.$$

To assess the confidence level of this result, we generate 30 statistically representative realizations of the dataset and compute the maximum anisotropy level for each realization, thus obtaining a reference distribution for comparison. By following this approach, we find that the observed anisotropy

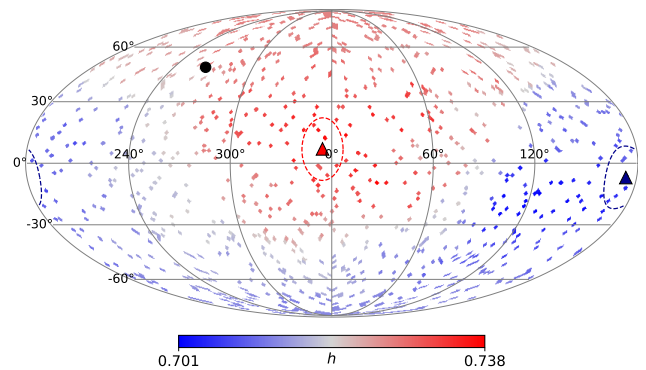


Fig. 9: HC method applied to CSP dataset with all 25 Cepheids calibrators in all directions. Panel show all-sky map of  $h$  for the 1000 directions investigated. Red and blue triangles mark the antipodal directions of the maximum anisotropy level for  $h$ . The black circle denotes the CMB dipole direction.

level corresponds to a statistical significance of  $2.5\sigma$ . It should be emphasized that this result only accounts for statistical uncertainties.

To account for systematic uncertainties, we adopt the approach from Uddin et al. (2024), where the systematic error is estimated as  $\sigma_h^{\text{sys}} = \frac{\sigma_M^{\text{sys}}}{2.17} h$ , where the systematic uncertainty in the absolute magnitude is obtained by subtracting the statistical uncertainty from the total uncertainty in quadrature. We take the total uncertainty from Table 8 of Uddin et al. (2024) being  $\sigma_M^{\text{stat+sys}} = 0.037$ , corresponding to the Cepheid calibration in the  $B$  band, and the statistical uncertainties are derived from our own fits. Following this procedure, we obtain a systematic uncertainty of  $\sigma_h^{\text{sys}} = 0.011$ , for both maximum and minimum directions. Consequently, the significance of the observed anisotropy is reduced to the  $1\sigma$  level, and the anisotropy is therefore not statistically compelling when the full uncertainty budget is taken into account.

We show in Figure 10 the corner plots of  $h_{\text{ALmax}}$  and  $h_{\text{ALmin}}$  for the CSP sample. The left panel shows results with statistical uncertainties only, while the right panel includes both statistical and systematic uncertainties. In each case, the plots display the joint probability of  $h$  and  $M$ , marginalized over the remaining nuisance parameters.

Similarly to the analysis performed with the Pantheon+ sample, we investigate the stability of the inferred anisotropy directions using the CSP dataset by propagating the intrinsic scatter of SNe Ia through the full inference pipeline. In each Monte Carlo realization, every supernova is perturbed by a random intrinsic scatter term of amplitude  $\pm 0.11$  mag, that inducing variations in the inferred value of  $h$ .

Table 5 summarizes our four representative realizations. We find significant variations in the anisotropy directions relative to the unperturbed case, indicating that the inferred axes are not robust against statistical and systematic fluctuations. The recovered directions for these realizations are shown in Fig. 11, showing that the maximum anisotropy

Table 4: Maximum hemispherical anisotropy in the Hubble parameter for the CSP sample.

	Value	AL	Significance	
			Stat	Stat+Syst
$h_{AL_N}^{\max}$	$0.737 \pm 0.009$ (Stat) $\pm 0.011$ (Syst)	2.7AL	$2.5\sigma$	$1.0\sigma$
$h_{AL_S}^{\max}$	$0.703 \pm 0.009$ (Stat) $\pm 0.011$ (Syst)			

Table 5: HC method with four intrinsic-scatter realizations of the CSP sample. Maximum and minimum  $h$  values with sky coordinates  $(l, b)$  are listed for each realization.

Method	N	$h_{\max}$	$(l, b)_{h_{\max}}$	$h_{\min}$	$(l, b)_{h_{\min}}$
HC	1	$0.744 \pm 0.013$	(26.8, -10.7)	$0.722 \pm 0.009$	(206.8, 10.7)
	2	$0.774 \pm 0.010$	(156.8, -21.9)	$0.714 \pm 0.010$	(336.8, 21.9)
All Cepheids	3	$0.764 \pm 0.011$	(329.4, 16.0)	$0.748 \pm 0.010$	(149.4, -16.0)
	4	$0.733 \pm 0.010$	(125.1, -14.0)	$0.720 \pm 0.010$	(305.1, 14.0)

directions obtained with the HC method are weakly constrained. Despite this variability, the directions tend to align along an axis connecting the upper-left and lower-right regions of the galactic coordinate system. This apparent preference is consistent with the highly inhomogeneous sky distribution of CSP supernovae, which exhibit very limited coverage in the opposite (upper-right) region. Given that the HC method compares opposite hemispheres, this observational bias disfavors preferred axes intersecting poorly sampled areas. Therefore, the observed alignment is likely driven by the survey geometry rather than being a genuine cosmological signal.

Table 5 summarizes four CSP realizations generated by applying the corresponding intrinsic scatter perturbations. Our results show significant variations in the values of  $h$  and their associated directions when compared to the unperturbed case. This behavior suggests that the inferred anisotropy axes are not robust against statistical and systematic fluctuations.

Figure 11 shows the directions obtained from the realizations including this intrinsic scatter. For clarity, only four representative realizations are displayed. The wide spread of these directions suggests that the recovered maximum anisotropy directions with the HC method are weakly constrained.

## 6. Discussion

Though, in most of the studies mentioned in the introduction, it has not been fully tested the consistency in the direction of anisotropy of the SNe Ia, we find interesting what is done in Kazantzidis & Perivolaropoulos (2020). They start with the Pantheon sample which has 1048 SNe Ia that are quite non uniformly distributed with a strong dependence of datapoint location in the southern hemisphere in the longitude range  $[0^\circ, 180^\circ]$ . They select a subsample of 375 SNe Ia and distribute them more isotropically in the four quadrispheres (100 in the first three and 75 in the down right quadrisphere). Using this reduced data set, which is more uniformly distributed, they produce 100 simulated Pantheon subsamples using 1500 random directions to split it in two hemispheres. They identified the maximum magnitudes, finding opposite points in the maximum and minimum directions. They show in their Figure 8 (left) the points of maximum and minimum moving within the hemispheres with no preferent direction.

The previous work had the limitation in the Pantheon data of not having the calibration of distances. Pantheon+ has the advantage of being calibrated with the Cepheids from SH0ES. The magnitude  $\mathcal{M}$  is a combination that includes the absolute magnitude of SNe Ia M and the Hubble constant.

$$\mathcal{M} \equiv M + 5 \log_{10} \left[ \frac{c/H_0}{1 \text{ Mpc}} \right] + 25 \quad (11)$$

The  $\mathcal{M}$  is degenerate in M and  $H_0$ . In the study of evolution of M,  $\mathcal{M}$  varying with  $z$ , could be as well  $H_0$  varying with  $z$ . As the aim of this paper is exploring the evolution in  $z$ , the creation of more uniform samples in the sky is positive for the research.

While the work by Kazantzidis & Perivolaropoulos (2020), taking different samples of 100 SNe Ia in every quadrisphere in the sky, implies that the information on the position in the sky of this small samples will change, the work by Bengaly et al. (2024) fully redistributes an original Pantheon+ subsample (SNe Ia from  $0.01 < z < 0.1$ ) in an uniform distribution in the sky. They replace the original SN coordinates with random ones across the celestial sphere. They are interested in the directional dependence of the parameter  $q_0$ . The sample selected by them includes 697 SNe Ia from Pantheon+. They make a Hemisphere Comparison, but taking caps of  $60^\circ$  in the sky, and assume an M absolute magnitude of the SNe Ia fixed, and  $H_0$  fixed across directions in the sky. With the original sample they obtain an anisotropic level of  $\Delta q_0 = 3.06$ . When they redistribute in the sky the SNe Ia, they obtain a  $\Delta q_0 = 2.96$ . Thus, they conclude that there is no statistically significant indication for a breakdown of the cosmic isotropy hypothesis when testing  $q_0$ .

In our case, substituting SNe Ia and placing them in a different sky position would remove precisely variations in  $H_0$  linked to existing bulk flows created by inhomogeneities in mass distributions. Thus, we do not redistribute them in the sky, for this test of directional anisotropy, but we simply perturb the real sample with its real positions in the sky with a  $\delta H_{0,i}$  from the light curve method. What would remain can then be linked to important factors impacting on the calculation of local  $H_0$ , including precisely the underlying velocity fields.

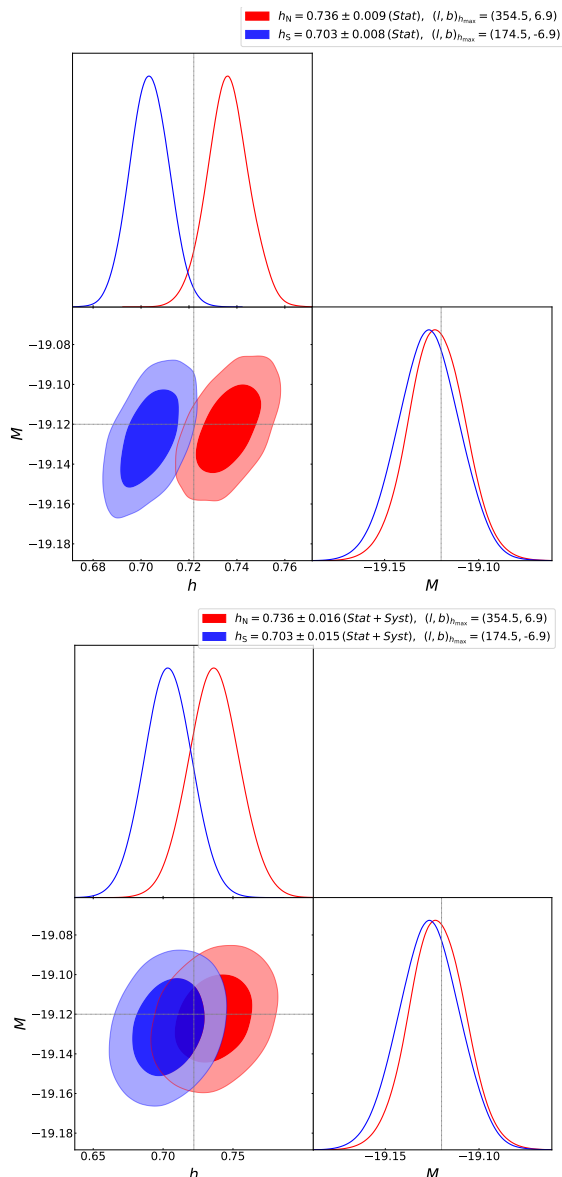


Fig. 10: Probability density contours for CSP from the HC method for the free parameters  $h$  and  $M$ , corresponding to the maximum anisotropy level in  $h$  found along the opposite directions  $(l, b)_N = (354.5 \pm 12.2, 6.9 \pm 15.1)$  and  $(l, b)_S = (174.5 \pm 12.2, -6.9 \pm 15.1)$ . Left: statistical uncertainties only. Right: statistical and systematic uncertainties. Vertical and horizontal lines indicate the parameter values reported by Uddin et al. (2024) from their analysis of the full CSP sample using Cepheid calibrators in the B band.

We have seen that perturbing with the individual  $H_{0,i}$ , the directional methods point to arbitrary anisotropy directions in the sky.

A number of works that use the HC method have referred to the effect of having a sample inhomogeneously distributed in the sky as a limitation to judge on the anisotropy of the cosmological parameters. Deng and Wei (2018) provide an analysis using the HC method with the JLA compilation, a sample of only 740 SNe Ia (Betoule et al. 2014). They do as well the simulation of having 5000 SNe Ia distributed with a given anisotropy (Pole-centralize or Equator-centralized)

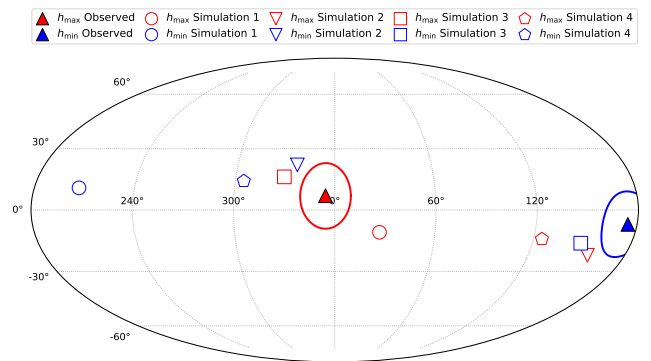


Fig. 11: Results of simulations including an intrinsic scatter of  $\sigma_{int} = 0.11$  mag for CSP.

and find that the HC method is able to recover well the previously assigned anisotropy direction, whereas another directional method named dipole fitting method fails. This exercise is aimed at simulating what will happen with the Nancy Grace Roman Space Telescope SNe Ia, at their time called WFIRST. However, they do not specify the error assigned in the determination of the distance to SNe Ia with the Roman telescope (WFIRST in their paper). Such error is expected to be smaller than the present one limited by the current use of the lightcurve SN Ia method. However, the SNe Ia survey planned with Roman will not be an all sky survey. Another study is presented by Chang and Lin (2015), who analyze the Union2 dataset, a sample of 557 SNe Ia (Amanullah et al. 2010) using the HC method. These last authors find that the preferred directions inferred can differ significantly, even pointing in nearly opposite directions when considering subsets of the data. Through Monte Carlo simulations, they remark that the HC results are highly sensitive to the non-uniform angular distribution of SNe Ia, which can bias the inferred anisotropy signal. A different approach to test isotropy is presented by Javanmardi et al. (2015), who analyze the Union2.1 compilation (Suzuki et al. 2012). Unlike the standard HC technique, their method does not assume any specific form of anisotropy and is conceptually similar to the RF method. The sky is scanned by defining conical regions around different directions, and the SNe Ia within each cone are used to fit the cosmological parameters. Repeating this procedure over the full sky yields maps of  $\Omega_\Lambda$ , under the assumption of spatial flatness, together with a nuisance parameter absorbing  $H_0$  and calibration effects. By varying the cone size ( $\theta = 90^\circ, 60^\circ, 30^\circ$ ), they also test possible scale dependence of anisotropic signals. Their results are consistent with statistical fluctuations, and no robust evidence for anisotropy is found. While some directions show mild alignment with the CMB dipole direction, these features are not significant once sky coverage is taken into account, concluding that the Union2.1 sample is compatible with isotropy. Zhao et al. (2019) applied the HC method to the original Pantheon compilation, covering the redshift range  $0.01 < z < 2.3$ . Since the original Pantheon sample is not calibrated with Cepheid distances, the analysis is performed using relative distance moduli. Using the HC method they report a preferred direction at  $(l, b) \approx (123.1^\circ, 4.8^\circ)$ , with a statistical significance of  $2.1\sigma$  in  $\Omega_m$ . However, they show that this signal is predominantly driven by the low- $z$  subset, indicating that it does not reflect a global anisotropic feature of the full dataset. They find a

strong correlation between the inferred anisotropy map and the highly non-uniform angular distribution of SNe Ia in the Pantheon sample. Overall, their results suggest that any apparent anisotropy is highly sensitive to survey inhomogeneities. This conclusion is consistent with the limitations discussed in previous works. These articles point to the fact that the identification of a cosmic preferred direction is data-dependent and should therefore be interpreted with caution.

Given the dependence on the size of the sample, now we will only refer to the largest SNe Ia data set analysed for anisotropy: the Pantheon+ sample (Brout et al. 2022, Scolnic et al. 2022). We have studied the factors that lead to conflicting confidence level in a claim of anisotropy in Pantheon+. We can study here the results from Hu et al. (2023), which use Pantheon+ and claim anisotropy at the  $3.15\text{--}3.96\sigma$  level. A major effect is to include the small amount from the 42 Cepheid calibrators that belong to each region of the fitting instead of all Cepheids. This makes very small the amount of Cepheids for the calibration. Using only local Cepheids per region in the sky makes the distance estimates highly sensitive to statistical fluctuations due to the reduced subsample, and it could spuriously suggest anisotropy. If done in this way, the outcome of the anisotropy in  $H_0$  from the SNe Ia reveals the anisotropy of the Cepheids. Using the full calibrators sample provides a more robust result (as presented here). It also lowers the significance level to let the sample establish the absolute magnitude  $M$  of the SNe Ia. If  $M$  is fixed a priori, with no allowance for any error, one forces a more significant result. In most papers  $M$  is let as a free parameter, but it is not the case in Hu et al. (2023), for instance. Just these changes (avoiding to introduce a false Cepheid anisotropy, and avoiding an a priori fixed  $M$ ) bring the statistical significance to  $< 1\sigma$ , instead of  $3\sigma$ .

McConville & Colgáin (2023) treat  $M$  as a free parameter. They impose, though, a redshift cutoff of  $z < 0.7$ . We find a comparable  $h$  map distribution (noting that they use equatorial coordinates, whereas we adopt galactic coordinates). The region of  $h_{max}$  coincides with the direction of the CMB dipole. McConville & Colgáin. (2023) report angular variations in  $H_0$  with a significance of  $1.9\sigma$ , interpreting their results as either a breakdown of isotropy or a statistical fluctuation among Cepheid-hosted supernovae. Even though we detect some level of anisotropy, reproducing their analysis with the RF method, our analysis indicates that this signal diminishes to  $1\sigma$  when accounting for the full Cepheid calibration sample, that suggesting that the apparent anisotropy is definitely more likely due to limitations in the completeness of the Cepheid calibrating sample.

Zhou, Dodelson & Scolnic (2025) have explored as well perturbations in the map of individual  $H_{0,i}$  of Pantheon+ SNe Ia consistent with statistical noise and sample variance. In their research, they consider the full sky  $\delta$  map. The perturbation is larger than the one consider here, which was limited to the intrinsic error of the SNe Ia lightcurve method. Zhou, Dodelson & Scolnic (2025) address as well the uncertainty of the Hubble constant as measured in the CMB,  $\delta_{CMB}$ , constructing residual maps of each sky patch with  $\delta_{CMB} = h(p)/h_{Planck} - 1$ . They find no hint of anisotropy or correlation between early and late-Universe expansion with SNe Ia and CMB.

Here we do not aim at studying the very early anisotropy of the Hubble parameter, but the late-Universe one, and how the dozens of different applications of the region fitting or hemisphere comparison approaches miss the point that the direction marked by this method has no significant relevance in the context of the present SNe Ia samples. The angular variation in the sky of  $4 \text{ km s}^{-1} \text{ Mpc}^{-1}$  simply reflects half the scatter of values across different points in the galactic coordinate map. It is important to keep in mind that this value is the basic limitation in measuring  $H_0$  from SNe Ia light curves.

When generating random realizations of the Pantheon+ and CSP datasets that include this intrinsic scatter, we find that the same RF and HC methods often yield significantly different preferred directions. Although the number of realizations is limited due to computational constraints, these results indicate that the directions identified by these methods are not stable in front of intrinsic scatter uncertainties. Therefore, this result should be considered when attempting to pinpoint a precise direction of anisotropy with such methods.

The inferred anisotropy level is fully consistent with isotropy at the current level of precision. The SNe Ia individual  $H_0$  should have smaller errors than the present ones. Then, it might be possible to find at a reasonable confidence level any evidence of anisotropy.

## 7. Conclusions

Our comprehensive Pantheon+ analysis, accounting for both statistical and systematic uncertainties, shows a weak departure from isotropy that vanishes when all Cepheid calibrators are considered in the maximum and minimum directions of  $h$ . Consequently, we find no compelling indication of a directional preference in the Hubble parameter. We find, as it can be seen by analyzing the variation of  $H_0$  along galactic coordinates, that there is no pattern privileging any direction of anisotropy. From one neighboring point to the next,  $H_{0,i}$  is expected to vary at least  $4 \text{ km s}^{-1} \text{ Mpc}^{-1}$ . We have found hints that the RF and HC methods can produce arbitrary directional anisotropy results. We performed the exercise of randomly distributing a point-to-point variation of  $\pm 4 \text{ km s}^{-1} \text{ Mpc}^{-1}$  ( $\pm 8 \text{ km s}^{-1} \text{ Mpc}^{-1}$  is the one observed in the CSP and Pantheon+ datasets,  $\pm 4 \text{ km s}^{-1} \text{ Mpc}^{-1}$  corresponding to the intrinsic error of the lightcurve method,  $\sigma_{int} = 0.11 \text{ mag}$ ), and in each run of the RF and HC methods a different direction of anisotropy was obtained. This argues against the robustness of the directional results found by those methods when the scatter is large, as it is the case in our analysis. Likewise, our statistical analysis using the CSP dataset, which probes the low- $z$  regime, shows a  $\sim 2\sigma$  deviation. When the statistical and systematic errors are taken into account, the anisotropy signal drops to the  $1\sigma$  level. We highlight that with the RF and HC methods it is not possible to draw a definite conclusion about the presence or absence of anisotropy in  $H_0$  at present, with Pantheon+ and other SNe Ia samples. More robust constraints may require combining this approach with independent probes. Achieving robust constraints with SNe Ia will require lower SNe Ia uncertainties, uniform sky coverage, and larger accurate SNe Ia samples that might be soon available for rigorously testing the foundations of the standard cosmological model.

*Acknowledgements.* We acknowledge support from the High Performance Computing (HPC) resources of the DRAGO supercomputer, affiliated with the Spanish National Research Council (CSIC) PR-L and A.Q-E acknowledge support from grant PID2021-123528NB-I00, from the the Spanish Ministry of Science and Innovation (MICINN).

## References

- Amanullah, R., Lidman, C., Rubin, D., et al. 2010, *ApJ*, 716, 712
- Andrade, U., Bengaly, C.A.P., Santos, B., J. S. & Alcaniz, J.S. 2018, *ApJ*, 865, 119
- Antoniou, I., & Perivolaropoulos, I. 2010, *JCAP*, 12, 012
- Asmussen, S., & Glynn, P.W. 2007, *Stochastic Simulation: Algorithms and Analysis* (Springer, New York, NY)
- Bengaly, C.A.P., Alcaniz, J.S., & Pigozzo, C. 2024, *PhRvD*, 109, 123533
- Betoule, M., Kessler, R., Guy, J., et al. 2014, *A&A*, 568, A22
- Brout, D., Scolnic, D., Popovic, B., et al. 2022, *ApJ*, 938, 110
- Camphuis, E., Quan, W., Balkenhof, L., et al. 2026, *PhRvD*, 113, 083504
- Carr, A., Davis, T.M., Scolnic, D., et al. 2022, *PASA*, 39, e046
- Chang, Z., & Lin, H.-N. 2015, *MNRAS*, 446, 2952
- Chapra, S.C. 2017, *Numerical Methods for Engineers*, 7th ed. (McGraw-Hill Education, New York, NY)
- Colin, J., Mohayaee, R., Rameez, M., & Sarkar, S. 2019, *A&A*, 631, L13
- Deng, H.-K., & Wei, H. 2018, *PhRvD*, 97, 123515
- Di Valentino, E., Levi Said, J., Riess, A.G., et al. 2025, *PDU*, 49, 101965
- Foreman-Mackey, D., Hogg, D.W., Lang, D., & Goodman, J. 2013, *PASP*, 125, 306C
- Freedman, W.L., Madore, B.F., Hatt, D., et al. 2019, *ApJ*, 882, 34
- Golub, G.H., & Loan, C.F.V. 1996, *Matrix Computations*, 3rd ed. (Johns Hopkins University Press, Baltimore, MD)
- Hamuy, M., Folatelli, G., Morrell, N.T., et al. 2006, *PASP*, 118, 2
- Hicken, M., Challis, P., Jha, S., et al. 2009, *ApJ*, 700, 331
- Hsiao, E.Y., Phillips, M.M., Marion, G.H., et al. 2019, *PASP*, 131, 014002
- Hu, J.P., Wang, Y.Y., Hu, J., & Wang, F.Y. 2024, *A&A*, 681, A88
- Javanmardi, B., Porciani, C., Kroupa, P., & Pflamm-Altenburg, J. 2015, *ApJ*, 810, 47
- Johnson, R.A., & Wichern, D.W. 2014, *Applied Multivariate Statistical Analysis*, 6th ed. (Pearson, Upper Saddle River, NJ)
- Kalus, B., Schwarz, D.J., Seikel, M., & Wiegand, A. 2013, *A&A*, 553, A56
- Kazantzidis, L., & Perivolaropoulos, I. 2020, *PhRvD*, 102, 023520
- Lewis, A. 2019, arXiv e-prints, arXiv:1910.13970
- Lin, H.-N., Wang, S., Chang, Z., & Li, X. 2016, *MNRAS*, 456, 1881
- Lopes, M., Bernui, A., Franco, C., & Avila, F. 2024, *ApJ*, 967, 47
- McConville, R., & Ó Colgáin, E. 2023, *PhRvD*, 108, 123533
- Mandel, K.S., Narayan, G., & Kirshner, R.P. 2011, *ApJ*, 731, 120
- Murakami, Y., Riess, A.G., Stahl, B.E., et al. 2023, *JCAP*, 2023, 046
- Nikakhtar, F., Ayromlou, M., Baghran, S., et al. 2018, *MNRAS*, 478, 5296
- Perlmutter, S., Aldering, G., Goldhaber, G., et al. 1999, *ApJ*, 517, 565
- Peterson, E.R., Kenworthy, D.W., Scolnic, D., et al. 2022, *ApJ*, 938, 112
- Phillips, M.M., Contreras, C., Hsiao, E.Y., et al. 2019, *PASP*, 131, 014001
- Riess, A.G., Filippenko, A.V., Challis, P., et al. 1998, *AJ*, 116, 1009
- Riess, A.G., Yuan, W., Macri, L.M., et al. 2022, *ApJL*, 934, L7
- Riess, A.G., Li, S., Anand, G.S., et al. 2025, *ApL*, 992, L34
- Ruiz-Lapuente, P., Quintana-Estellés, A., González Hernández, J.I. Pastorello, A. 2025, arXiv e-prints, arXiv:2512.02391
- Schwarz, D.J., & Weinhorst, B. 2007, *A&A*, 474, 717
- Scolnic, D.M., Jones, D.O., Rest, A., et al. 2018, *ApJ*, 859, 101
- Scolnic, D., Brout, D., Carr, A., et al. 2022, *ApJ*, 938, 113
- Sorrenti, F., Durrer, R., & Kunz, M. 2023, *JCAP* 2023, 054
- Suzuki, N., Rubin, D., Lidman, C., et al. 2012, *ApJ*, 746, 85
- Tsagas, C.G., Perivolaropoulos, L., & Asvesta, K. 2026, *PhR*, 1178, 1
- Tully, R.B., Kourkchi, E., Courtois, H.M., et al. 2023, *ApJ*, 944, 94
- Uddin, S.A., Burns, C.R., Phillips, M.M., et al. 2024, *ApJ*, 970, 72
- Vincenzi, M., Brout, D., Armstrong, P., et al. 2024, *ApJ*, 975, 86
- Watkins, R., & Feldman, H.A. 2025, arXiv e-prints, arXiv:2512.03168
- Whitford, A.M., Howlett, C., & Davis, T.M. 2023, *MNRAS*, 526, 3051
- Yuan, S., & Eisenstein, D.J. 2019, *MNRAS*, 486, 708
- Zhao, D., Zhou, Y., & Chang, Z. 2019, *MNRAS*, 486, 5679
- Zhou, A.J., Dodelson, S., & Scolnic, D. 2025, arXiv e-prints, arXiv:2506.14878
- Zuntz, J., Paterno, M., & Jennings, E. 2015, *A&C*, 12, 45